Structure, Vol. 10, 933–942, July, 2002, ©2002 Elsevier Science Ltd. All rights reserved. PII S0969-2126(02)00778-5

Molecular Basis of Mitomycin C Resistance in *Streptomyces*: Structure and Function of the MRD Protein

T.W. Martin,[1] Zbigniew Dauter,[2] Yancho Devedjiev,[1] Peter Sheffield,[1] Filip Jelen,[3] Min He,[4] David H. Sherman,[4] Jacek Otlewski,[3] Zygmunt S. Derewenda,[1] and Urszula Derewenda[1,5]

[1]Department of Molecular Physiology and Biological Physics
University of Virginia
Health Sciences System
Charlottesville, Virginia 22908

[2]National Cancer Institute
Frederick and National Brookhaven Laboratory
Building 725A-X5
Upton, New York 11973

[3]Institute of Biochemistry and Molecular Biology
University of Wrocław
50-137 Wrocław
Poland

[4]Department of Microbiology and BioTechnology Institute
University of Minnesota
Minneapolis, Minnesota 55455

Summary

Mitomycin C (MC) is a potent anticancer agent. *Streptomyces lavendulae*, which produces MC, protects itself from the lethal effects of the drug by expressing several resistance proteins. One of them (MRD) binds MC and functions as a drug exporter. We report the crystal structure of MRD and its complex with an MC metabolite, 1,2-*cis*-1-hydroxy-2,7-diaminomitosene, at 1.5 Å resolution. The drug is sandwiched by π-stacking interactions of His-38 and Trp-108. MRD is a dimer. The βαββββ fold of the MRD molecule is reminiscent of methylmalonyl-CoA epimerase, bleomycin resistance proteins, glyoxalase I, and extradiol dioxygenases. The location of the binding site is identical to the ones in evolutionarily related enzymes, suggesting that the protein may have been recruited from a different metabolic pathway.

Introduction

Mitomycin C (MC, M_W 331) is a highly cytotoxic, DNA-reactive antibiotic produced by *Streptomyces lavendulae* [1]. Approved by the Food and Drug Administration as an anticancer drug in 1974, MC has been used widely and continues to be of use in the treatment of bladder, head and neck, cervical, gastric, pancreatic, and colon cancers [2–4]. In its prodrug form (Figure 1A), MC does not bind to DNA and becomes biologically active only after reductive conversion to a short-lived and highly reactive quinone methide [5–7]. The latter compound lacks the methoxide substituent, and the aziridine ring is opened, conferring high reactivity on the sp^2 carbon C1. In this activated form, MC monoalkylates the 2-NH2 group of guanines in the minor groove via the C1 carbon and may form intra- and interstrand cross-links at both the C1 and C10 positions [8] (Figure 1B). Since cells halted in G2 phase will die, rapidly proliferating cells are especially vulnerable to this attack. The bioreductive activation often requires NAD(P)H as the electron donor and is enzymatically catalyzed [9]. Since many detoxification enzymes specifically bind quinones, MC can effectively "hijack" enzymes that normally neutralize free radicals in the cell. As a paradigm for a bioreductive alkylating agent, MC has attracted substantial attention [2, 10].

Reoxidation of the products of reductive metabolism of MC leads to the formation of 2,7-diaminomitosene (2,7-DAM) (nucleophilic pathway) or a mixture of 1,2-*cis* and 1,2-*trans*-1-hydroxy-2,7-diaminomitosenes (1-hydroxy-2,7-DAMs) (Figure 1C). Structurally similar to quinone methide, this compound is much less cytotoxic than MC, even though it binds DNA and may alkylate it following an additional reductive event [9, 11, 5]. Interestingly, acid hydrolysis of MC also results in a similar conversion of MC, but the predominant product is 1,2-*cis*-1-hydroxy-2,7-DAM, not a mixture of *cis* and *trans* isomers [12].

Two proteins in *S. lavendulae* that are products of the *mcrA* and *mrd* genes have been shown to confer resistance to MC [13–15]. MCRA (54 kDa) has a covalently bound FAD cofactor and acts by oxidizing the activated (reduced) MC before it can bind DNA [16]. In contrast, MRD, a 14 kDa, single chain protein, interacts with MC itself and functions as a component of a drug-exporting pathway [15]. Recent work indicates that MRD works in conjunction with a membrane-associated protein (MCT) to expel MC from the cell [17]. Both the *mrd* and *mct* genes are found within the MC biosynthetic gene cluster in *S. lavendulae* [18].

Clinical research suggests potential applications for proteins with functions similar to those of MRD and MCRA. A genetic therapy protocol involving the bioreductively-activated alkylating agent CB-1954 was recently approved for phase I/II studies by the FDA [19]. The protocol involves transfection of the gene for an activating enzyme (nitroreductase) selectively to tumor cells, thereby sensitizing them to chemotherapy. Healthy somatic cells, which would only be exposed to the prodrug form of CB-1954, could therefore be spared harmful side effects. A future application of proteins similar to MRD and/or MCRA might conceivably work in an inverse manner, providing healthy cells with specific resistance to MC [20] and allowing for a much more aggressive treatment of tumors than is presently possible.

Structural characterization of the MRD resistance protein was pursued to explore the molecular basis of MC

[5]Correspondence: ud3a@virginia.edu

Key words: mitomycin C; antibiotic resistance; SAD; anomalous diffraction; domain swapping; π stacking

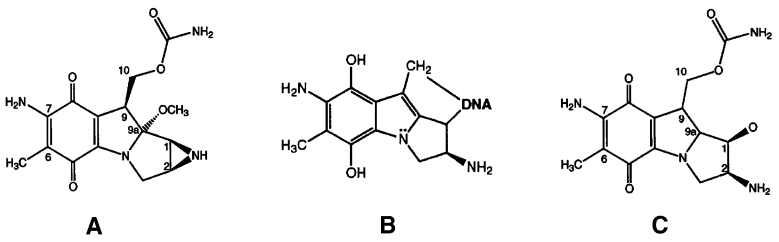

Figure 1. The Chemistry of Mitomycin C

(A) Mitomycin C (NSC 26980 in the National Cancer Institute database).

(B) Formation of covalent DNA cross-links occurs via bonding at C1 and C10.

(C) 1,2-*cis*-1-hydroxy-2,7-diaminomitosene.

drug binding and transport. Herein we describe the molecular architecture of the native MRD protein and the structural details of the complex of MRD with 1,2-*cis*-1-hydroxy-2,7-DAM, which binds to MRD with an association constant that is five times higher than that of MC. MRD is a dimer, with each monomer containing a tandem repeat of $\beta\alpha\beta\beta\beta$ modules. Two different modes of dimer formation are observed, suggesting a domain-swapping event. The drug binding sites are located in deep clefts on the opposite sides of the molecule and formed either by the curvature of the β sheet within a monomer or, when domain swapping occurs, by two $\beta\alpha\beta\beta\beta$ modules from adjacent monomers. The drug is sandwiched by π-stacking interactions between the protonated imidazole of His-38 and the indole ring of Trp-108.

Results and Discussion

Structure Determination and Model Quality

MRD was overexpressed in *E. coli*, purified, and crystallized as described in Experimental Procedures. The use of the MAD phasing technique based on SeMet was limited due to the presence of only one Met residue. Therefore, we designed a double mutant in which Leu-19 and Leu-25 were replaced by methionine residues. Crystals of the SeMet containing double mutant diffracted beyond 1.3 Å resolution (see Table 1). For experimental phasing, we used a single data set collected at the absorption peak of Se (0.979 Å) from a crystal soaked for two days in the mother liquor containing MC (see Experimental Procedures). The positions of the three methionine residues were readily determined and allowed for the calculation of preliminary phases. The initial model was created using ARP/wARP [21], which automatically built 110 out of a total of 130 residues, and refined with SHELXL [22]. Additionally, a complete data set to 1.5 Å was first collected from a crystal of the wild-type and unliganded protein.

Though the quality of the model based on the 1.3 Å SeMet dataset was good, the density presumed to correspond to the ligand was deemed unsatisfactory. Therefore, the experiment was repeated, and 1.5 Å resolution data were collected from another SeMet-containing crystal that was soaked for a longer period in the presence of MC. Subsequent refinement against these data revealed full occupancy for a bound ligand, which proved to be 1,2-*cis*-1-hydroxy-2,7-DAM (see below for further details of the chemistry). The final, refined model of the complex is derived from this 1.5 Å data set.

In all three crystal structures, a single monomer occupies the asymmetric unit of the C2 unit cell, and two monomers form a close association with the resultant 2-fold axis of the MRD dimer corresponding to the crystallographic dyad. This is consistent with our gel filtration results (data not shown), which indicate that a dimer is the predominant species in solution. For all three refined models, each monomer contains residues 3–130, inclusive, with the region containing residues 65–71 being comparatively less well ordered. Residues in this region were not included until final refinement, for reasons explained below. There are 153, 161, and 158 ordered water molecules included in the final models for the ligand-bound, apo form, and 1.3 Å resolution structures, respectively. In the case of the complex structure, a molecule of 1,2-*cis*-1-hydroxy-2,7-DAM was modeled into residual positive difference electron density and included late in refinement. The known geometry of the quinone ring was used as a restraint, while the remaining moieties were restrained using standard bond lengths and angles.

The quality of the models, as judged by stereochemical criteria, is high (see Table 2), and PROCHECK [23] analysis indicates that approximately 95% of the residues in the final models are in the most favored regions with no outliers.

Table 1. X-Ray Experimental Data

	Apo-MRD	Partial Ligand Occupancy	Full Ligand Occupancy
Resolution (Å)	1.5	1.3	1.5
Number of reflections			
Total	74,125	119,032	66,770
Unique	17,820	27,880	18,054
Redundancy	4.15	4.26	3.64
Completeness (%)	99.9 (99.4)[a]	99.9 (99.6)	99.9 (100.0)
R_{sym} (%)[b]	3.4 (33.5)	6.8 (34.2)	4.6 (30.1)
I/σ ratio	36.1 (3.6)	13.9 (3.4)	26.3 (4.0)

[a] The numbers in parentheses describe the relevant value for the last resolution shell.

[b] $R_{sym}\ \Sigma|I_i - \langle I\rangle|/\Sigma I$, where I_i is the intensity of the ith observation and $\langle I\rangle$ is the mean intensity of the reflections.

Table 2. Refinement Details

	Partial Ligand Occupancy	Full Ligand Occupancy	Apo-MRD
Resolution used in final refinement (Å)	10.0–1.3	10–1.5	10.0–1.5
R_{cryst}/R_{free} (%)[a]	16.1/22.9	13.6/20.9	16.8/23.4
Rmsd from target bond lengths (Å)/bond angles (°)	0.017/2.09	0.018/2.14	0.016/1.8
Rmsd from <B> (Å^2) overall	2.11	2.38	2.41
Average B factors (Å^2)			
Main chain atoms	19.28	22.25	23.26
Side chain atoms	23.57	26.90	26.27
Waters	39.63	42.76	44.8

[a] $R_{cryst} = \Sigma|F_o - F_c|/\Sigma|F_o|$, where F_c is the calculated structure factor.

MRD Is a Member of a Diverse Family of βαββββ Proteins

MRD is an oblong dimer with dimensions of roughly 50 × 40 × 30 Å (Figure 2B). Each monomer is made up of an eight-stranded β sheet, with each sheet comprised of two βαββββ motifs (domains) packed edge to edge, so that the first strands of the two modules are associated in an antiparallel manner. The basic topology in each domain is a four-stranded β sheet (defined as +1, +4, −3, and +2) with an α helix connecting strands 1 and 2 (Figure 2A). Domain A consists of residues 3–53, and domain B consists of residues 74–130, while residues 54–73 form the connecting region, including a short α helix. In spite of lack of identifiable sequence similarity between the two domains, their tertiary structures are very close. A superposition of the two modules in MRD yields 38 pairs of Cα atoms with a root-mean-square (rms) difference of 1.6 Å.

Tandem βαββββ motifs have been observed in several other proteins with diverse functions. They originally included the bleomycin resistance protein from *Streptoalloteichus hindustanus* (*Sh*Ble) [24], two extradiol dioxygenases [25, 26], and glyoxalase I [27]. These structures were quickly recognized to be representative of a larger family [28]. More recently, additional members were described: the bleomycin resistance proteins found in *Streptomyces verticillus* (BLMA) [29] and on transposon Tn5 in *E. coli* (BLMT) [30], a methylmalonyl-coenzyme A epimerase (MMCE) from *P. shermanii* [31], and several more dioxygenases and glyoxalases [32–35].

Of particular interest is the structural similarity between MRD and the bleomycin resistance proteins (BRPs). As with MC, bleomycin is an antibiotic and DNA cleaving agent but is chemically unrelated. However, there is some identifiable, albeit low, amino acid se-

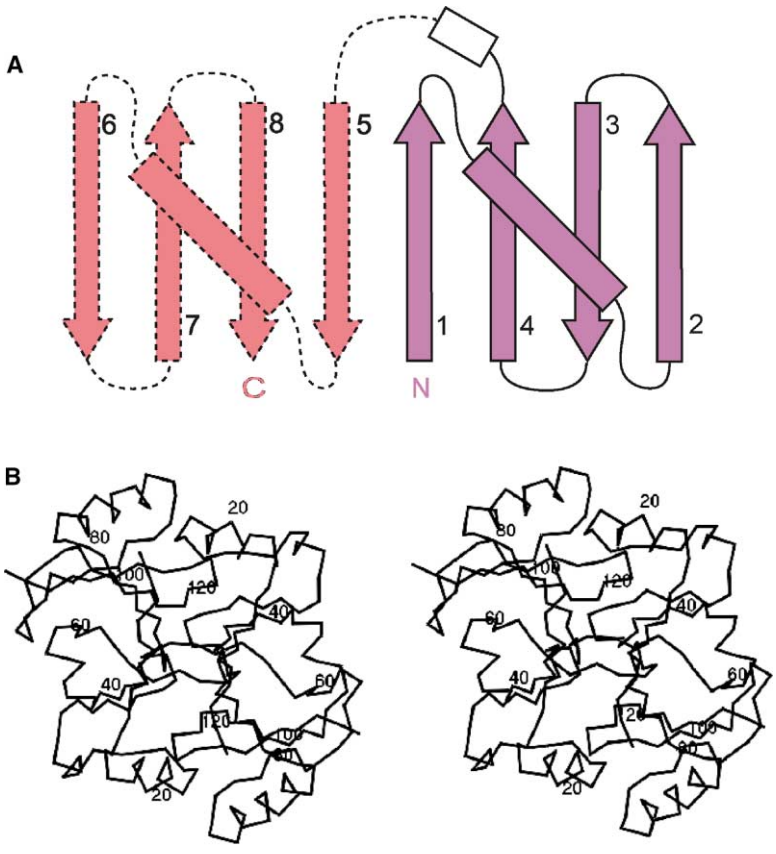

Figure 2. The Structure of MRD Protein

(A) Topology of the MRD monomer. Domain A, pink; domain B, red.

(B) Stereoview of the Cα tracing of the MRD dimer.

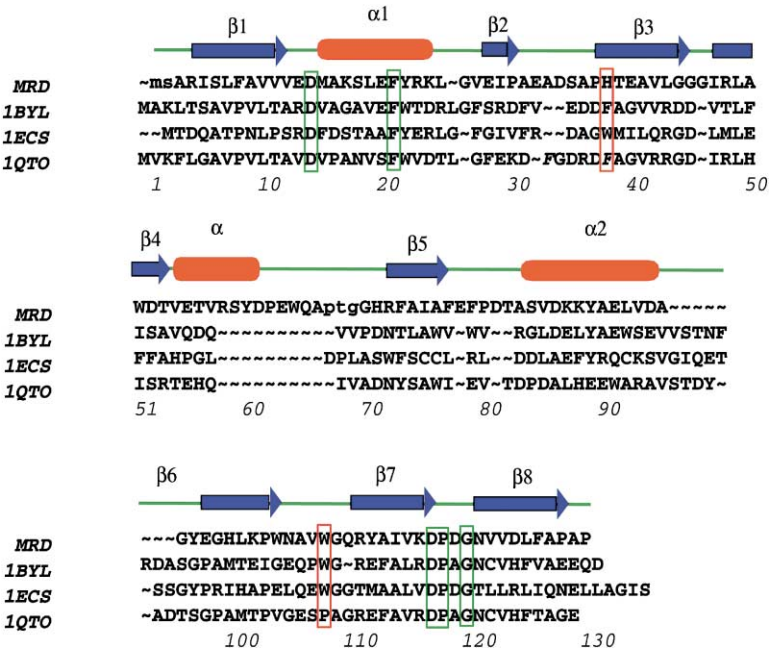

Figure 3. Structure-Based Sequence Alignment of MRD with Bleomycin Resistance Proteins ShBle (1BYL), BLMT (1ECS), and BLMA (1QTO)

The two key residues involved in sequestering the drug are boxed in red; the five invariant residues in the sequences are boxed in green.

quence similarity between MRD and the BRPs (Figure 3). This similarity extends to the level of structure: the first βαββββ motifs of MRD and *Sh*Ble (1BYL in PDB) superpose with 28 Cα atom pairs yielding an rms difference of 2.4 Å, while the C-terminal motifs match even better, with 53 Cα pairs, i.e., essentially the entire domains, superposing with an rms difference of 1.9 Å. Even more striking is the similarity between MRD and BLMA (1QTO): the first domains superpose with 42 Cα pairs with an rms difference of 1.8 Å, and the second yield 53 pairs and an rms difference of 1.9 Å.

Other proteins in this family are also structurally similar. The MMCE molecule displays particular similarity to MRD in the second βαββββ motif, for which a superposition of 49 Cα atoms yields an rms difference of 1.6 Å. The prevailing pattern, noted by previous authors [28, 31], is that the N-terminal modules superpose on each other better than on the C-terminal motifs and vice versa.

Although in all three structures the MRD dimer consists of two pairs of domains A and B related by crystallographic symmetry, alternative connectivities between these domains give rise to two topologically distinct forms generated by a 3D domain-swapping phenomenon. Our electron density indeed corroborates that both species are present, albeit each crystal form selects preferentially for one. In form I, observed in wild-type unliganded MRD, each monomer consists of a continuous eight-stranded sheet, and the back to back interface between the eight-stranded sheets establishes the interface between the two monomers. In form II, found in both drug-bound SeMet-containing crystals, each monomer contributes half of each of the two eight-stranded sheets in the dimer (Figure 4). The structural differences between these forms result from a simple change in the linker connecting the two domains. In form I, residues 67–69 form two turns, which face each other as symmetry-related structures. In form II, proline 67 and threonine 68 are in an extended conformation and form two linear strands going in opposite directions.

The family of proteins to which MRD belongs is recognized for a history of gene duplication and domain-swapping events [28, 31, 36]. The original gene duplication event led to the βαββββ tandem structure, which appears to require dimerization for stability. Owing to the nature of the dimer, in which the connecting linkers are close together, two alternative modes of dimerization are possible. Interestingly, while MMCE conforms to one of these (form I), BRPs and human glyoxalase exemplify the other (form II), and the two groups were contrasted in literature as evidence of evolutionary 3D domain swapping [28]. Further duplication is observed in dioxygenases, where two tandems are covalently linked to form a sequential 4-fold repeat of the βαββββ module. The MRD structures, on the other hand, appear to suggest that the domain-swapping events may be dynamic, so that the two forms may coexist in solution, while crystallization selectively isolates either one or the other. Whether this is a consistent feature of other proteins in the family remains to be seen.

The Bound MC Derivative Is 1,2-*cis*-1-Hydroxy-2,7-DAM

MRD crystals turn pink when soaked for a few days in mother liquor solution containing crystalline MC. Because MC is purple, with a visible absorbance spectrum showing a single peak at 360 nm, the pink color suggested the appearance of a compound closely related to 2,7-diaminomitosene, with a characteristic absorbance peak at 313 nm. The initial 1.3 Å data set, derived from crystals soaked for two days, yielded a region of density suggestive of a bound ligand, albeit of poor quality. The 1.5 Å data set, obtained from a crystal soaked for four days, yielded very well-defined electron density for the bound drug. We noted that there was no electron density associated with the methoxy substituent at C9a of MC, and the region corresponding to C9 carbon clearly showed the flattened sp^2 hybridization, with the substit-

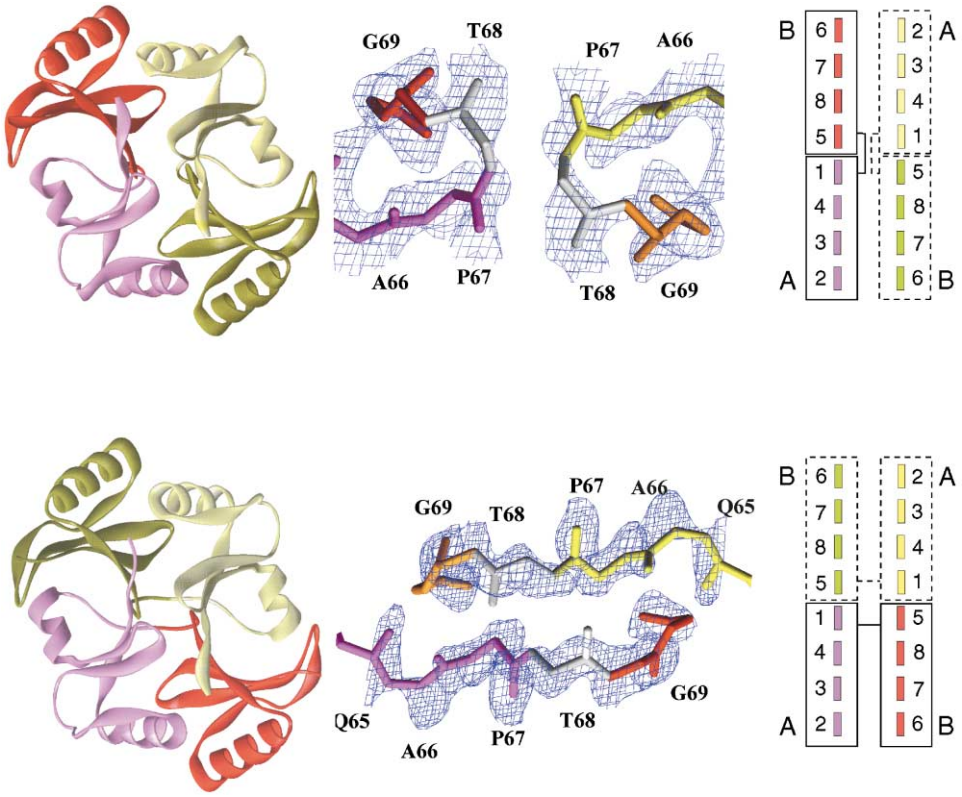

Figure 4. The Two Topological Forms of the MRD Dimer

Form I and form II are on the left, close-ups of their respective "crossover" region are in the center, and schematic diagrams of the β strands (represented perpendicular to the page) are on the right. In form I, each β sheet is created by a single monomer (A connected to B), while, in form II, each sheet is composed of the A domain from one monomer and the B domain of the other (A connected to B′). For each protein, one monomer is shown with its first domain pink and its second domain red (the convention used in Figure 2), while the other monomer is shown with its first domain yellow and its second domain gold. The electron density shown is from omit maps, with the three relevant residues removed for several rounds of least-squares refinement.

uent in the plane of the quinone, rather than the tetrahedral sp^3 geometry associated with MC (Figure 5A). Further, there was clear evidence (as judged from the electron density) of the opening of the aziridine ring with two substituents in positions 1 and 2 in *cis* configuration. All these details are consistent with 1,2-*cis*-1-hydroxy-2,7-DAM, and not MC, being bound to MRD. For final refinement a set of model constraints, based on the known crystal structure of MC, was used [37].

Since 1,2-*cis*-1-hydroxy-2,7-DAM is a reaction product derived from either reduction or acid hydrolysis of MC, we decided to determine whether MRD has catalytic properties under the conditions used to generate crystals. We monitored the stability of MC in solution by measuring absorption spectra in the visible wavelength range. The hydrolysis of MC to 1-hydroxy-2,7-DAM is accompanied by a change of spectrum with excellent isosbestic points at 330 and 240 nm, indicating that no intermediates are involved [12], and the reaction is easily followed by spectrophotometric means. Our data (data not shown) indicate that MC is stable in 100 mM MES buffer at pH 6.0 in both the presence and absence of MRD. However, the addition of 65% saturated ammonium sulfate results in the hydrolysis of MC to 1,2-*cis*-1-hydroxy-2,7-DAM over a period of hours to days, again with and without addition of MRD. We conclude that under the conditions of our experiments, MRD is not involved in the hydrolytic transformation of MC, which occurs in solution due to general acid/base catalysis.

The structural analysis of MRD shows that its drug binding site is located within a deep cleft formed by the curved eight-stranded β sheet, with the flat hydroquinone moiety of 1-hydroxy-2,7-DAM packing tightly into a "slot" created by the side chains of residues His-38 and Trp-108 (see below for further details). The presence of a tryptophane in the binding site allowed us to measure the dissociation constants (K_d) for MC and 1-hydroxy-2,7-DAM using fluorimetric titration. The dissociation constant for MC determined in this way is 31 μM, while that for 1-hydroxy-2,7-DAM shows tighter binding—6.3 μM. This shows that the integrity of the aziridine ring and the methoxide group of MC are not required for efficient binding and that MRD is capable of binding both MC and its immediate reaction product.

The Drug Binding Site

The symmetry-related binding pockets are located on opposite sides of the dimer. In form I, each binding cavity is created by the bent, or "cup", structure of the eight-stranded β sheet of each monomer. In form II, the

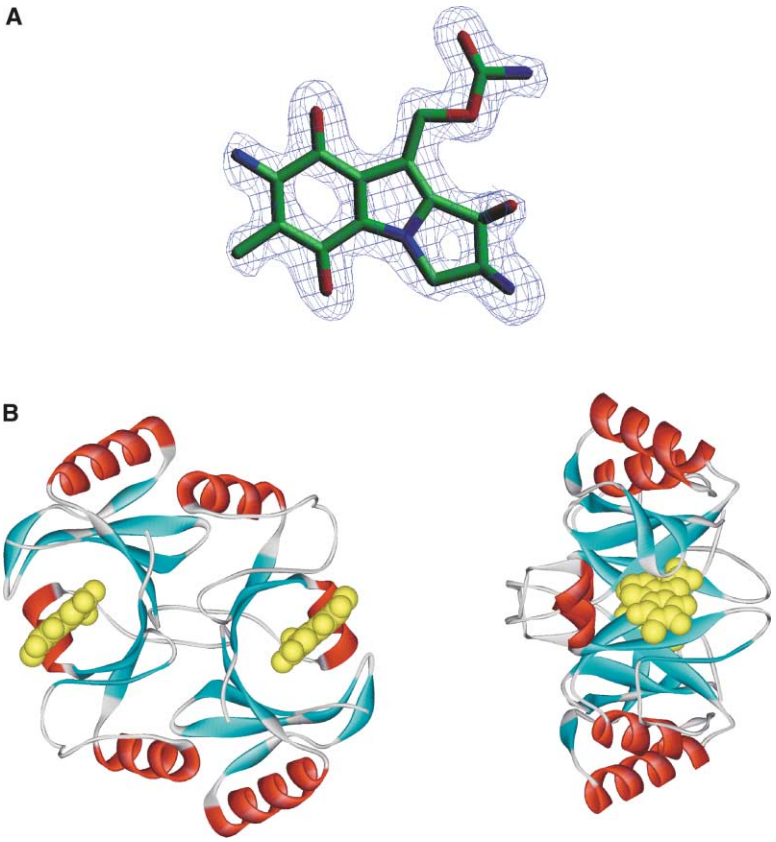

Figure 5. The Binding of 1,2-*cis*-1-Hydroxy-2,7-DAM to MRD

(A) Electron density and a model of the bound 1,2-*cis*-1-hydroxy-2,7-DAM molecule. The density shown was generated using an omit map, with ligand model removed before several rounds of refinement.

(B) Two views of the bound form of the MRD dimer, again in form II, with helices in red and β sheets in light blue. The DAM molecule is depicted in yellow.

β sheet is created from four strands from each monomer, and the binding pocket is therefore also composed partly from one monomer and partly from the other (Figure 5B). Regardless of the topological differences between the two forms, the chemistry of the binding site remains the same.

The most noticeable feature of the substrate binding region is the outer rim, where the flat hydroquinone moiety of DAM packs tightly into a slot created by the imidazole of His-38 and the indole ring of Trp-108. It is interesting to note that His-38 remains protonated and charged, due to two interactions with carboxylates, one with Asp-52 through Nδ1 and one with Glu 40 via Nϵ2. Both are short H bonds with 2.6 Å distances. The imadazole (His-38) and the five-membered portion of the indole (Trp-108) face each other, with their centers approximating a common axis for both rings. The hydroquinone moiety is sandwiched between these two rings, so that the C8a carbon packs between the centers of the rings. A nearly straight line can be drawn from the Cϵ1 carbon of the histidine through the C8a carbon of the quinone to the Cγ carbon of the tryptophan. The total separation is 7.0 Å, with the C8a situated almost precisely in between, at a distance of 3.5 Å from the other two atoms (Figure 6A).

The region of the DAM molecule corresponding to the location of the aziridine ring in MC makes contact with residues in the interior of the protein, while the opposite side is exposed to bulk solvent. The C9 substituent is held in place by a set of hydrogen bond interactions, notably the terminal N14 nitrogen with Tyr-112 and the terminal O13 oxygen with Gln-110, and by two water molecules within the cavity. The specific binding of this amidoacetate group appears important because the dissociation constant for MC of the Y112F mutant, in which one of the hydrogen bonds is removed, is 0.4 mM, an order of magnitude higher than that of the wild-type protein. There is also an H bond network involving the hydroxy oxygen (designated O0 in the model) and the amino nitrogen N1 (which is an aziridine nitrogen in MC). This network involves a water molecule that forms bonds with both the O0 oxygen and the N1 nitrogen. Two other residues, Tyr-60 and Asp-52, each form a hydrogen bond with the N1 nitrogen as well. The negative charge on Asp-52 is not critical because the D52N mutant binds MC with affinity virtually identical to the wild-type protein.

The overall arrangement of residues in wild-type unliganded MRD is not significantly different from the drug-bound form. The distance between His-38 and Trp-108 is slightly larger in the native form, so the cleft between them appears to narrow when packed with the DAM quinone. The space occupied by the ligand in the complex is filled by approximately eight ordered water molecules in the unliganded form of the protein. The overall arrangement of the hydrogen bonding network, particularly one involving Asp-52 and Tyr-60, can be see in Figure 6B. The bound 1,2-*cis*-1-hydroxy-2,7-DAM does not induce any significant structural changes in the MRD protein.

Comparison with BRPs

As already pointed out, MRD shares its overall tertiary and quaternary structure with BRPs, which also have a

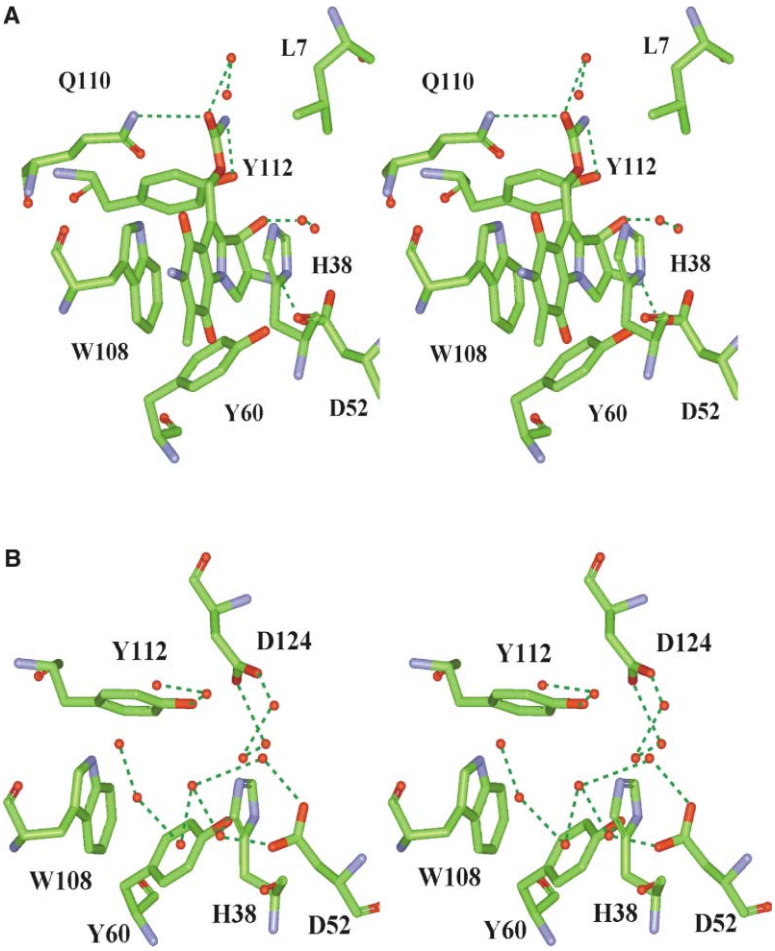

Figure 6. The Stereochemical Details of the Binding Site

(A) Stereoview of DAM within the binding region.

(B) Stereoview of the water structure inside the binding cavity of the native form.

pair of symmetric cavities that serve as binding sites, but there are substantial differences between the two target drugs. Bleomycin, the ligand for BRPs, is a far larger molecule than MC and chemically unrelated. It contains several chemical groups, including bithiazole, methylvalerate threonine linker, and metal binding and sugar moieties. Recently, a crystallographic study revealed the structural details of the BLMT-Bm complex [30]. The linker, metal binding, and sugar groups of Bm interact with numerous amino acids within a shallow surface groove, but the bithiazole moiety, made up of two five-membered rings, is sequestered between two tryptophanes, i.e., Trp-99 and Trp-35, which correspond to Trp-108 and His-38 of MRD. The loops containing these crucial residues have virtually identical stereochemistries in the two proteins, although the details of the interaction with ligand vary (Figure 7). Trp-108 of BLMT has the indole ring rotated nearly 180° around χ_2, as compared to MRD, and Trp-35 has the five-membered ring nearly overlapping with the imidazole of His-38 when the two models are overlapped. The distance between the two parallel indoles is about 7 Å. The first thioazole group of Bm interacts only with Trp-108, while the second thiozole is sequestered by both indoles. BLMT binds Bm with a dissociation constant of 32 nM, but it is not known whether bithiazole binds on its own and with what affinity. Thus, even though the nature of the ligand is very different, the mode of drug binding by the bleomycin resistance proteins and MRD is very similar.

Biological Implications

The study reported in this paper describes the high-resolution crystallographic study of the MRD resistance protein in complex with a derivative of the cancer drug mitomycin C. The MRD dimer is believed to be part of a drug transport system that shuttles the MC molecule out of the drug-producing organism *Streptomyces lavendulae*. The protein is a member of a larger family of enzymes and drug binding molecules characterized by a conserved βαββββ motif as a principle module. The quinone moiety of the bound 1,2-*cis*-1-hydroxy-2,7-DAM is sandwiched between the imidazole of His-38 and the indole of Trp-108. Affinity measurements show that both mitomycin C and 1-hydroxy-2,7-DAM bind with similar dissociation constants (in the μM range). The binding mode is similar to that observed for the bleomycin resistance protein, where a bithiazole moiety is sequestered between two tryptophan residues that occupy sites equivalent to those of Trp-108 and His-38 in MRD. This suggests that the βαββββ proteins are promiscuous in their interactions with ligands and could be engineered to bind a diverse set of planar molecules of biological importance.

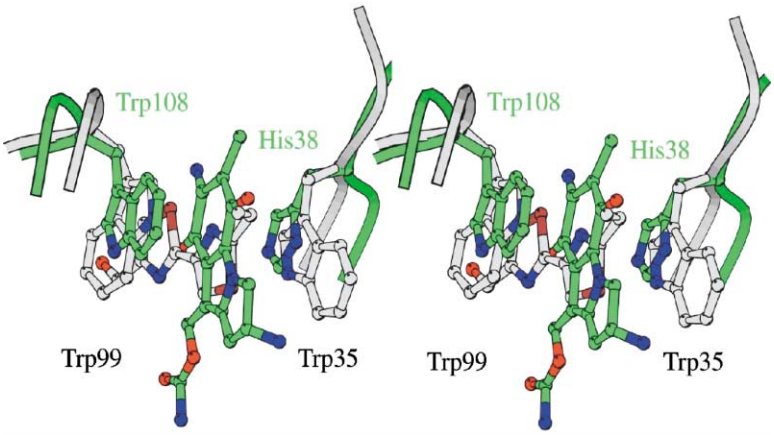

Figure 7. The Comparison of the BLMT and MRD Binding Sites

The 1,2-*cis*-1-hydroxy-2,7-DAM molecule and the bithiazole of BM are shown with the α carbons of the two sequestering amino acids superposed on each other.

Experimental Procedures

Expression of MRD in *E. coli*

The *mrd* gene was subcloned into an expression vector used to create a GST fusion protein with an rTEV proteolytic cleavage site (pGST-Parallel1) [38]. Aggregation difficulties with the MRD-GST fusion protein led us to test samples using size exclusion chromatography. This provided early evidence that MRD was a dimer and that higher-order oligomers of MRD-GST were responsible for aggregation. The *mrd* gene was then subcloned into a His_6-tag expression vector (pHis Parallel1) [38]. The sequence-verified plasmid was transformed into *E. coli* BL21(DE3) (Novagen). The cells were grown at 37°C in 1 liter of LB broth containing 100 μg/ml ampicillin to an OD_{600} of 0.6–0.8, and expression was initiated by the addition of IPTG to a final concentration of 1 mM. The culture was grown for an additional 3 hr at 37°C. The cells were harvested by centrifugation at 8,000 × g for 10 min at 4°C. The pellet was resuspended in ice-cold His buffer (5 mL/g; 300 mM NaCl and 50 mM Tris-HCl [pH 8.5]) and sonicated on ice using five 30 s bursts with a 5 min cooling period between each burst. The cellular debris was pelleted by centrifugation at 11,500 × g for 30 min at 4°C, and supernatant was used for further purification of MRD.

Purification of MRD

Purification of His_6-tagged MRD was carried out by standard methods with slight modifications. The supernatant was passed through a column containing 5 ml of preequilibrated (His buffer) Ni^{2+}-NTA agarose to bind the His_6-tagged MRD, and the resin was washed with 2 liters of His buffer at 4°C. The bound protein was recovered with elution buffer containing 250 mM imidazole (pH 8.5). The His_6-tag was cleaved with 1 μl of rTEV protease (Gibco) per milliliter of sample for 48 hr at room temperature. A 10,000 MWCO Slide-a-Lyser cassette (Pierce) was used for dialysis against 4 liters of His buffer to remove imidazole and the cut His_6-tag. The dialyzed solution was passed through a column containing 5ml of Ni^{2+}-NTA agarose to remove both uncut protein and rTEV protease. The protein was concentrated to ~3 mg/mL by using an Amicon 8050 ultrafiltration unit with a YM 10 membrane (10,000 MWCO; Millipore).

Mutagenesis and Preparation of SeMet Samples

The L19M and L25M mutations used to introduce additional methionine residues for phasing purposes, as well as the D52N and Y112F mutations designed to probe the specificity of the binding site, were prepared using QuikChange protocol. All constructs were verified by direct sequencing prior to further use. To obtain SeMet samples, the auxotrophic strain B834 was transformed with the pHIS plasmid. Cultures were grown in LeMaster medium, with selenomethionine replacing methionine. The expression protocol paralleled that of the native protein described above, with the important exception that 1 day was required for the culture to reach the necessary optical density, instead of several hours. The purification protocol was likewise identical, with the exception that the rTEV cleavage reaction took nearly a week to run to completion, instead of two days.

Binding Assays

Dissociation constants (K_d) were determined by fluorimetric titration of MRD wild-type and its two mutant forms (D52N and Y112F) with increasing concentrations of drug (MC or DAM). To determine the dissociation constant, increasing amounts of the drug were added to a constant concentration of the MRD. In each case eight to ten data points were collected. Experiments were done in duplicate at 20°C using an FP-750 spectrofluorometer (Jasco) under the following conditions: λ excitation = 280 nm, λ emission = 342 nm, and excitation and emission slit width = 5 nm. MC or 1-hydroxy-DAM (2 μM–0.7 mM) were added to 1200 μl of 1.8 μM MRD in 100 mM MES (pH 6.0). The residual protein fluorescence was measured after 100 min incubation. The dissociation constants were determined as described previously [39]. The protein concentration was estimated using the molar absorbance coefficient ϵ_{280} = 28,226 M^{-1} cm^{-1} for MRD WT and MRD D52N and ϵ_{280} = 27,028 M^{-1} cm^{-1} for MRD Y112F, calculated from the number of Trp and Tyr residues in the MRD molecule [40]. The MC concentration contained in solution was estimated using the molar absorbance coefficient ϵ_{367} = 21,840 M^{-1} cm^{-1}. The DAM concentration was determined using the molar absorbance ϵ_{313} = 10,189 M^{-1} cm^{-1}, determined by the total acidic hydrolysis of the known amount of MC.

Crystallization and Sample Preparation

Crystallization was accomplished using protein at 3 mg/ml concentration in 55% ammonium sulfate and 100 mM MES at pH 6.0. Native crystals were small and frequently twinned. Addition of β-octylglucoside to a final concentration of 0.05% slowed down crystal growth and reduced twining. SeMet crystals grew in similar conditions, with the exception of a small increase in ammonium sulfate (65%). The SeMet crystals grew more slowly (3–4 weeks) and were typically single and larger, with maximal dimensions of 0.25 × 0.15 × 0.15 mm. SeMet crystals were soaked in mother liquor with increased ammonium sulfate content (100 mM MES and 75% ammonium sulfate) containing crystalline mitomycin C and NADH at a concentration of approximately 1–2 mM each. NADH was used because of previously published data, which suggested that MC binding by MRD is NADH dependent [16]. However, our present data show that, in the presence of NADH, MRD binds MC with a dissociation constant of 24.1 μM, i.e., within experimental error the same as in its absence. Soaks without NADH produced pink MRD crystals in comparable time. Native and soaked SeMet crystals were flash frozen using mother liquor solution with high (70%) ammonium sulfate concentration and 12% v/v glycerol.

Structure Solution and Model Refinement

Data were collected at beamline X9B of the National Synchrotron Light Source (Brookhaven National Laboratory) using a Quantum 4 ADSC CCD area detector. The apo-MRD data set was collected to a resolution of 1.5 Å, the partial soak to a resolution of 1.3 Å, and the full soak to 1.5 Å. A total of 180 frames were collected for the high-resolution (1.3 Å) data set, 1° rotation each. The unit cell was identified as C2; a = 42.5 Å, b = 65.3 Å, c = 45.3 Å, and β = 105.6°

(V_m = 1.96 Å^3/Da). Data were reduced using HKL [41]. Details are shown in Table 1. Anomalous differences from the data set processed to 1.3 Å were used to locate the positions of the three selenium atoms using SHELXS [22]. This substructure was used in MLPHARE, and the phases were modified in DM as implemented in CCP4 [42] using standard settings. The resulting density was of very high quality and was used for automatic model building using wARP [21], which placed 110 out of 130 total residues. This model was used as a starting point in the refinement against all three data sets, initially done with REFMAC [43]. The only significant difference between the models occurs at residues 66–70, which is the crucial connecting region between domains. For each data set, refinement was done with and without models of these residues to demonstrate that the connecting density is not an artifact. Final refinement was done using SHELXL [22], which was also used for final placement of waters for each model. (For those parts of the DAM model that differ from MC, standard bond angles and distances were used, as no DAM crystal structure is available.)

Figures

The figures were prepared using O [44], SETOR [45], and WebLab ViewerPro (MSI).

Acknowledgments

We thank Dr. Mirka Dauter for her help with the collection of the native MRD data set, Dr. Daniel Krowarsch for help with fluorescence experiments, and Josh Durham and Mary Lewis for technical assistance. This study was funded in part by NIH grant CA81172 to D.H.S. and U.D., as well as by NATO Collaborative Linkage grant LST.CLG.977818 to Z.S.D. and J.O.

Received: January 31, 2002
Revised: April 22, 2002
Accepted: April 29, 2002

References

1. Hata, T., Sano, Y., Sugawara, R., Matsumae, A., Kanamorei, K., Shima, T., and Hoshi, T. (1956). Mitomycin, a new antibiotic from *Streptomyces*. J. Antibiot. (Tokyo) *9*, 141–146.
2. Tomasz, M. (1995). Mitomycin C: small, fast and deadly (but very selective). Chem. Biol. *2*, 575–579.
3. Crooke, S.T., and Bradner, W.T. (1976). Mitomycin C: a review. Cancer Treat. Rev. *3*, 121–139.
4. Bradner, W.T. (2001). Mitomycin C: a clinical update. Cancer Treat. Rev. *27*, 35–50.
5. Kumar, G.S., He, Q.-Y., Behr-Ventura, D., and Tomasz, M. (1995). Binding of 2,7-diaminomitosene to DNA: model for the precovalent recognition of DNA by activated mitomycin C. Biochemistry *34*, 2662–2671.
6. Iyer, V.N., and Szybalski, W. (1964). Mitomycins and porfiromycin. Science *145*, 55–58.
7. Lin, A.J., Coby, L.A., and Sartorelli, A.C. (1972). Quinones as anticancer agents: potential bioreductive alkylation agents. Cancer Chemother. Rep. *4*, 23–25.
8. Tomasz, M., Lipman, R., Chowdary, D., Pawlak, J., Verdine, G.L., and Nakanishi, K. (1987). Isolation and structure of a covalent cross-link adduct between mitomycin C and DNA. Science *235*, 1204–1208.
9. Tomasz, M., and Lipman, R. (1981). Reductive metabolism and alkylating activity of mitomycin C induced by rat liver microsomes. Biochemistry *20*, 5056–5061.
10. Tomasz, M., Chawla, A., and Lipman, R. (1988). Mechanism of monofunctional and bifunctional alkylation of DNA by mitomycin C. Biochemistry *27*, 3182–3187.
11. Palom, Y., Belcourt, M.F., Kumar, G.S., Arai, H., Kasai, M., Sartorelli, A.C., Rockwell, S., and Tomasz, M. (1998). Formation of a major DNA adduct of the mitomycin metabolite 2,7-diaminomitosene in EMT6 mouse mammary tumor cells treated with mitomycin C. Oncol. Res. *10*, 509–521.
12. McClelland, R.A., and Lam, K. (1985). Kinetics and mechanism of the acid hydrolysis of mitomycins. J. Am. Chem. Soc. *107*, 5182–5186.
13. August, P.R., Flickinger, M.C., and Sherman, D.H. (1994). Cloning and analysis of a locus (*mcr*) involved in mitomycin C resistance in *S. lavendulae*. J. Bacteriol. *176*, 4448–4454.
14. August, P.R., Rahn, J.R., Flickinger, M.C., and Sherman, D.H. (1996). Inducible synthesis of the mitomycin C resistance gene product (MCRA) from *S. lavendulae*. Gene *175*, 261–267.
15. Sheldon, P.J., Johnson, D.A., August, P.R., Liu, H., and Sherman, D.H. (1997). Characterization of a mitomycin-binding drug resistance mechanism from the producing organism, *Streptomyces lavendulae*. J. Bacteriol. *179*, 1796–1804.
16. Johnson, D.A, August, P.R., Shackleton, C., Liu, H.-w., and Sherman, D.H. (1997). Microbial resistance to mitomycins involves a redox relay mechanism. J. Am. Chem. Soc. *119*, 2576–2577.
17. Sheldon, P.J., Mao, Y., He, M., and Sherman, D.H. (1999). Mitomycin C resistance in *Streptomyces lavendulae* includes a novel drug-binding-protein-dependent export system. J. Bacteriol. *181*, 2507–2512.
18. Mao, Y., Varoglu, M., and Sherman, D.C. (1999). Molecular characterization and analysis of the biosynthetic gene cluster for the antitumor antibiotic mitomycin C from Streptomyces lavendulae NRRL 2564. Chem. Biol. *6*, 251–263.
19. Chung-Faye, G., Palmer, D., Anderson, D., Clark, J., Downes, M., Baddeley, J., Hussain, S., Murray, P.I., Searle, P., Seymour, L., et al. (2001). Virus-directed, enzyme prodrug therapy with nitroimidazole reductase: a phase I and pharmacokinetic study of its prodrug, CB1954. Clin. Cancer Res. *9*, 2662–2668.
20. Belcourt, M.F., Penketh, P.G., Hodnick, W.F., Johnson, D.A., Sherman, D.H., Rockwell, S., and Sartorelli, A.C. (1999). Mitomycin resistance in mammalian cells expressing the bacterial mitomycin C resistance protein MCRA. Proc. Natl. Acad. Sci. USA *96*, 10489–10494.
21. Perrakis, A., Morris, R., and Lamzin, V.S. (1999). Automated protein model building combined with iterative structure refinement. Nat. Struct. Biol. *6*, 458–463.
22. Sheldrick, G.M., and Schneider, T.K. (1997). SHELXL: high resolution refinement. Methods Enzymol. *277*, 319–343.
23. Laskowski, R.A., McArthur, M.W., Moss, D.S., and Thornton, J.M. (1993). PROCHECK: a program to check the stereochemical quality of protein structures. J. Appl. Crystallogr. *26*, 282–291.
24. Dumas, P., Bergdoll, M., Cagnon, C., and Masson, J. (1994). Crystal structure and site-directed mutagenesis of a bleomycin resitance protein and their significance for drug sequestering. EMBO J. *13*, 2483–2492.
25. Han, S., Eltis, L.D., Timmis, K.N., Muchmore, S.W., and Bolin, J.T. (1995). Crystal structure of the biphenyl-cleaving extradiol dioxygenase from a PCB-degrading *Pseudomonas*. Science *270*, 976–980.
26. Senda, T., Sugiyama, K., Narita, H., Yamamoto, T., Kimbara, K., Fukuda, M., Sato, M., Yano, K., and Mitsui, Y. (1996). Three-dimensional structures of free form and two substrate complexes of an extradiol ring-cleavage type dioxygenase, the BphC enzyme from *Pseudomonas* sp. strain KKS102. J. Mol. Biol. *255*, 735–752.
27. Cameron, A.D., Olin, B., Ridderstrom, M., Mannervik, B., and Jones, T.A. (1997). Crystal structure of human glyoxylase I—evidence for gene duplication and 3D domain swapping. EMBO J. *16*, 3386–3395.
28. Bergdoll, M., Eltis, L.D., Cameron, A.D., Dumas, P., and Bolin, J.T. (1998). All in the family: structural and evolutionary relationships among three modular proteins with diverse functions and variable assembly. Protein Sci. *8*, 1661–1670.
29. Kawano, Y., Kumagai, T., Muta, K., Matoba, Y., Davies, J., and Sugiyama, M. (2000). The 1.5 Å crystal structure of a bleomycin resistance determinant from bleomycin-producing Streptomyces verticillus. J. Mol. Biol. *295*, 915–925.
30. Maruyama, M., Kumagai, T., Matoba, Y., Hayashida, M., Fuji, T., Hata, Y., and Sugiyama, M. (2001). Crystal structures of the transposon Tn*5*-carried bleomycin resistance determinant uncomplexed and complexed with bleomycin. J. Biol. Chem. *276*, 9992–9999.
31. McCarthy, A.A., Baker, H.M., Shewry, C.S., Patchett, M.L., and

Baker, E.N. (2001). Crystal structure of methylmalonyl-coenzyme A epirerase from *P. shermanii*: a novel enzymatic function on an ancient metal binding scaffold. Structure *9*, 637–646.

32. Serre, L., Sailland, A., Sy, D., Boudec, P., Rolland, A., Pebay-Peyroula, E., and Cohen-Addad, C. (1999). Crystal structure of the *Pseudomonas fluorescens* 4-hydroxyphenylpyruvate dioxygenase: an enzyme involved in the tyrosine degradation pathway. Structure *7*, 977–988.
33. Kita, A., Kita, S., Fujisawa, I., Inaka, K., Ishida, T., Horiike, K., Nozaki, M., and Miki, K. (1999). An archetypical extradiol-cleaving catecholic dioxygenase: the crystal structure of catechol 2,3-dioxygenase (metapyrocatechase) from *Pseudomonas putida* mt-2. Structure *7*, 25–34.
34. Saint-Jean, A.P., Phillips, K.R., Creighton, D.J., and Stone, M.J. (1998). Active monomeric and dimeric forms of Pseudomonas putida glyoxalase I: evidence for 3D domain swapping. Biochemistry *29*, 10345–10353.
35. He, M.M., Clugston, S.L., Honek, J.F., and Matthews, B.W. (2000). Determination of the structure of *Escherichia coli* glyoxalase I suggests a structural basis for differential metal activation. Biochemistry *39*, 8719–8727.
36. Cameron, A., Olin, B., Ridderstrom, M., Mannervk, B., and Jones, T. (1997). Crystal structure of human glyoxalase I—evidence for gene duplication and 3D domain swapping. EMBO J. *16*, 3386–3395.
37. Arora, S.K. (1979). Structural investigations of mode of action of drugs. I. Molecular structure of mitomycin C. Life Sci. *24*, 1519–1526.
38. Sheffield, P.J., Garrard, S., and Derewenda, Z.S. (1999). Overcoming expression and purification problems of RhoGDI using a family of 'parallel' expression vectors. Protein Expr. Purif. *15*, 34–39.
39. Bulaj, G., and Otlewski, J. (1995). Ligand-induced changes in the conformational stability of bovine trypsinogen and their implications for the protein function. J. Mol. Biol. *247*, 701–716.
40. Pace, C.N., Vajdos, F., Fee, L., Grimsley, G., and Gray, T. (1995). How to measure and predict the molar absorption coefficient of a protein. Protein Sci. *4*, 2411–2423.
41. Otwinowski, Z., and Minor, W. (1997). Processing of X-ray diffraction data collected in oscillation mode. Methods Enzymol. *276*, 307–326.
42. (CCP4) Collaborative Computational Project 4. (1994). The CCP4 suite: programs for crystallography. Acta Crystallogr. D Biol. Crystallogr. *50,* 760–763.
43. Murshodov, G.N., Vagina, A.A., and Dodson, E.J. (1997). Refinement of macromolecular structures by the maximum-likelihood method. Acta Crystallogr. D Biol. Crystallogr. *53*, 240–255.
44. Jones, T.A., Zou, J.Y., Cowan, S.W., and Kjeldgaard, M. (1991). Improved methods for binding protein models in electron density maps and the location of errors in these models. Acta Crystallogr. A *47,* 110–119.
45. Evans, S.V. (1993). SETOR: hardware-lighted three-dimensional solid model representations of macromolecules. J. Mol. Graph. *11*, 134–141.

Accession Numbers

Atomic coordinates were deposited in the Protein Data Bank under accession codes 1KMZ (unliganded MRD) and 1KLL (MRD with bound 1,2-*cis*-1-hydroxy-2,7-diaminomitosene).